Discrete Complex Image Method With Spatial Error Criterion

E. P. Karabulut, *Student Member, IEEE*, Alper T. Erdogan, *Member, IEEE*, and M. I. Aksun, *Senior Member, IEEE*

***Abstract*—Since its first inception, the discrete complex image method (DCIM) has been criticized for the lack of a proper prediction algorithm of the error incurred during the process. Although the method has been improved and modified several times, not being able to input any prior specification or to get any meaningful assessment on the error deters computer-aided design developers and engineers from using it in the development of commercial software and in-house simulation tools. To remedy this shortcoming of the otherwise very popular DCIM, a weighted p-norm of the spatial-domain error is defined, and its mapping to the spectral domain is derived and proposed as the metric to be used in the implementation of the DCIM. Once this metric is incorporated into the latest three-level DCIM algorithm, used for the approximation of the spatial-domain Green's functions, it is observed that the weighted error-energy minimization in the spectral domain becomes equivalent to the one in the spatial domain. In addition to introducing an error criterion to the DCIM, the leakage problem, which is inherent to the semi-independent processing of subregions in multilevel implementations of the DCIM, is also addressed and eliminated, resulting in a further improvement of the algorithm and the end result.**

***Index Terms*—Closed-form Green's functions, discrete complex image method (DCIM), layered media.**

I. Introduction

GREEN'S functions play an important role in computational electromagnetics, as they help transform governing wave equations to integral equations [1]–[3], and in turn, facilitate the use of the well-known method of moments (MoM) in the analysis of printed structures in multilayered media [4]–[8]. Since the implementation of the MoM in the spatial-domain requires the knowledge of the spatial-domain Green's functions, computing the spatial-domain Green's functions from their analytically expressible spectral-domain counterparts requires the implementation of the Hankel transform, generally referred to as Sommerfeld integrals in the literature. It is very well known that direct numerical evaluation of the Sommerfeld integrals is a time-consuming and computationally expensive process due to its oscillatory and slowly decaying nature [9], [10]. However, with the introduction of the discrete complex image method (DCIM) [11], [12], a new approach has emerged to get the spatial-domain Green's functions more efficiently and also in closed forms. Starting from its first introduction up to the latest development, all proposed approaches based on the DCIM suffer from the fact that there is no proper error minimization in the spatial domain. As a result, even though some robust algorithms with very good approximate results have been developed, the accuracy of the method has always been questionable, and no high level confidence is established for the method [13]. In this paper, it is intended to develop an algorithm that would answer this long-standing shortcoming of the method.

In order to put things into perspective, a brief chronological overview of the development of DCIM-based methods for the computation of the spatial-domain Green's functions is provided below. Before the introduction of the DCIM, there was mainly one general approach for the evaluation of Sommerfeld-type integrals: numerical integration in conjunction with some transform techniques [9], [10], [14]. Since this approach can provide the value of the integral for a fixed spatial distance ρ one at a time, and because one needs to know the spatial-domain Green's functions for a range of spatial distances in order to use them in conjunction with the MoM, it was not considered to be efficient and suitable for that purpose. Therefore, the proposal for approximating the spatial-domain Green's functions in closed forms in [11] and [12] attracted much interest, and they were followed by a series of related work [15]–[31]. The original work [11] and its follow-up [12] proposed approximating the spectral-domain Green's functions in terms of complex exponentials, and transforming them into the spatial-domain analytically with the help of the Sommerfeld identity. Although the idea was quite innovative, its implementation was not as robust and efficient as desired, and because of that, the method was restricted for a rather narrow class of geometries, namely, for a thick slab backed by a ground plane. This was first followed by an extension that improved its coverage of geometries to multilayered structures [15], [16], and was then followed by a rather major extension that has significantly improved the efficiency and robustness of the method (with the introduction of the two-level algorithm [17]). Although the two-level DCIM, when coupled with the analytical inclusion of the surface wave contributions, provided very good approximations in closed forms for the spatial-domain Green's functions over a distance well beyond a few wavelengths from the source [23], [24], [32], the far-field behavior in the vicinity of interfaces for some configurations is not accurate. This was rightly attributed to the lack of the lateral wave contribution in the closed-form representation, as it was shown that these configurations dominantly support lateral waves in the far-field region [29]. Since

Manuscript received September 13, 2010; revised December 04, 2010; accepted December 22, 2010. Date of publication February 10, 2011; date of current version April 08, 2011. This work was supported in part by the Turkish Academy of Sciences (TUBA) under the Program for Awarding Outstanding Young Scientists (GEBIP) and in part by the Scientific and Technological Research Council of Turkey (TUBITAK) under Career Award 104E073.

The authors are with the Department of Electrical and Electronics Engineering, Koc University, 34450 Sariyer, Istanbul, Turkey (e-mail: ekarabulut@ku.edu.tr).

Color versions of one or more of the figures in this paper are available online at http://ieeexplore.ieee.org.

Digital Object Identifier 10.1109/TMTT.2011.2105275

0018-9480/$26.00 © 2011 IEEE

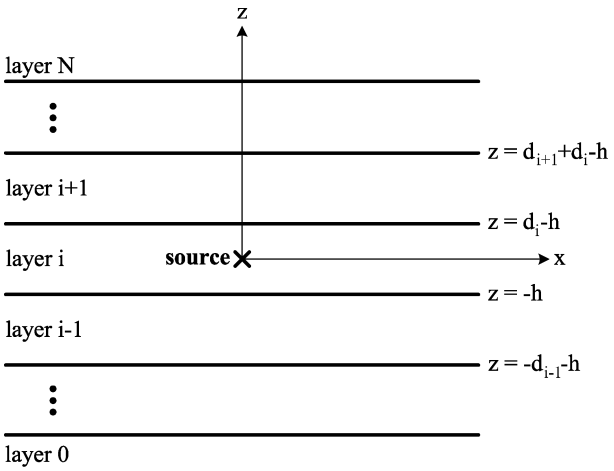

Fig. 1. General multilayer planar medium.

lateral waves in the spatial domain are due to the branch-point contributions in the spectral domain, the sampling path of the two-level DCIM has recently been modified in such a way that the new path passes very close to the branch point, and thus capture the branch-point contribution [31]. Consequently, by this latest version of the DCIM, it was demonstrated that all the natural wave constituents of a dipole in any configuration of planar layered media have been accounted for, and represented very accurately in the closed-form approximations of the spatial-domain Green's functions. Although such a powerful tool has been established to get the closed-form Green's functions quite efficiently, this would not be enough to increase confidence of computer-aided design (CAD) tool developers unless some sort of error metric is incorporated in the algorithm that would ensure the accuracy of the end result [13].

Since the proposed error metric will be implemented on the latest version of the DCIM, i.e., the three-level algorithm, it would be instructive to briefly review the key steps of the algorithm in Section II. It is followed, in Section III, by the introduction of errors in the spatial and the spectral domains, and their connections under the Hankel transformation. Section IV provides some numerical examples to validate the robustness, accuracy, and ease of implementation of the algorithm for a typical geometry, and some conclusions are drawn in Section V.

II. Brief Overview of DCIM

For the sake of illustration, consider a typical planar multilayered structure, as shown in Fig. 1, where the electromagnetic (EM) properties of the layers vary in the z-direction only.

It is well known that Green's functions for planar layered media are obtained recursively as closed-form expressions in the spectral domain, and can be transformed to the spatial domain by the following Hankel transform integral, also known as the Sommerfeld integral:

$$g(\rho) = \frac{1}{2\pi}\int_S dk_\rho k_\rho J_0(k_\rho\rho)G(k_\rho) \tag{1}$$

where g and G are the spatial- and spectral-domain Green's functions, respectively, J_0 is a zeroth-order Bessel function of the first kind, and S denotes the integration path defined over the first quadrant in the k_ρ-plane.

Since it is generally computationally intensive to evaluate Sommerfeld integrals using numerical integration algorithms, the DCIM has been developed to avoid this expensive step by mainly introducing two critical steps, which are: 1) approximate the closed-form spectral-domain Green's functions as the linear combinations of complex exponentials and 2) evaluate the Sommerfeld integrals in closed forms via the Sommerfeld integral identity

$$\frac{e^{-jk_0 r}}{r} = \int_S dk_\rho k_\rho J_0(k_\rho\rho)\frac{e^{-jk_z z}}{jk_z} \tag{2}$$

where $r = \sqrt{\rho^2+z^2}$ and $k_0 = \sqrt{k_\rho^2+k_z^2}$. As a result, the spatial-domain Green's functions can be written analytically as a sum of complex images

$$\underbrace{\frac{1}{4\pi}\sum_{l=1}^{M}\alpha^{(l)}\frac{e^{-jk_0 r^{(l)}}}{r^{(l)}}}_{g(\rho)} = \frac{1}{2\pi}\int_S dk_\rho k_\rho J_0(k_\rho\rho)\underbrace{\frac{1}{2jk_z}\sum_{l=1}^{M}\alpha^{(l)}e^{-\beta^{(l)}k_z}}_{G(k_\rho)} \tag{3}$$

where $r^{(l)} = \sqrt{\rho^2+(-j\beta^{(l)})^2}$ is a complex distance, due to which the method is referred to as the discrete complex image method (DCIM).

III. Connection Between Spectral- and Spatial-Domain Errors

As stated above, the main contribution of this paper is to propose a DCIM-based algorithm that minimizes the spatial-domain error. Remembering that the DCIM-based algorithms perform most of the error-prone processing in the spectral domain, to achieve this goal, one needs to develop some sort of mapping algorithm that would *transform* or *reflect* the error criterion in the spatial domain to the one in the spectral domain, as will be detailed below in this section.

Before getting into the details, it is necessary to set the stage for the development of the method by stating the problem formally as follows. For a given Hankel transform pair with a spatial-domain function $g(\rho)$ and its spectral-domain counterpart $G(k_\rho)$, construct an approximate spatial-domain function $\hat{g}(\rho)$ from the spectral-domain samples $(\{G(k_\rho{}^{(l)}) : k_\rho{}^{(l)} \in \mathcal{K}\}$ where $\mathcal{K}$ is a finite discrete ordered set with elements $\{k_\rho{}^{(1)}, k_\rho{}^{(2)}, \ldots, k_\rho{}^{(N)}\})$ such that the distance between the true spatial-domain function $g(\rho)$ and its estimate $\hat{g}(\rho)$ is minimized. According to the statement of the problem, it is necessary to define a distance between the two functions; as it is well known in functional analysis, all norms defined over the space of continuous variable functions qualify as valid

metric choices, among which the weighted p-norm is chosen as a suitable distance metric in this work, and defined by

$$C_p(e) = \left(\int_0^\infty w(\rho)|e(\rho)|^p d\rho \right)^{1/p} \tag{4}$$

where $w(\rho)$ is the nonnegative weighting function, $e(\rho)(= g(\rho) - \hat{g}(\rho))$ is the error function, and $p \geq 1$ is a rational number. The selection of the weighting function $w(\rho)$ and the constant p determines how error values at different locations contribute to the overall error magnitude, i.e., to the distance metric. To be more specific, one can choose the weighting function: 1) to give more weight to a certain region of interest by using an appropriate window function or 2) to enforce a similar signal to error magnitude ratios at all distances. Although the latter criterion requires the knowledge of the spatial-domain function $g(\rho)$, which is an unknown for the problem at hand, knowing or having some educated guess about its asymptotic behavior for large distances would be sufficient. For example, if $g(\rho) \propto 1/\rho^\alpha$ for large ρ, then a sensible choice for the weighting function would be $w(\rho) = \rho^{2\alpha}$ in order to achieve signal level dependent error weighting. Regarding the choice of the constant p, a typical choice is 2, which is a continuous extension of the Euclidean norm. This choice is mainly motivated by its algorithmic convenience, as well as the tractability of the corresponding analysis. In addition, it also plays an important role in terms of bridging the spatial-domain goals to the spectral-domain ones, as will be detailed below.

It is important to note that, unlike the Parseval relation in the Fourier transform, minimizing the 2-norm in the Hankel transform domain is not equivalent to minimizing the 2-norm in the spatial domain (with $w(\rho) = 1$). Therefore, the use of ordinary least squares (OLS) in the spectral domain, as it is the case in the standard DCIM procedure, is not justified from the error minimization point of view in the spatial domain. As a result, the cost function for the choice of $p = 2$ is written as

$$C_2(e) = \int_0^\infty w(\rho)|e(\rho)|^2 d\rho \tag{5}$$

where the power term 1/2 is dropped and $C_2(e)$ is referred to as the weighted error energy. Once the cost function is defined in the spatial domain, it needs to be mapped onto the spectral domain involving the error function $E(k_\rho)$, which is defined as the difference between the exact value of the spectral-domain expression and its approximation over the integration path S.

A. Parseval-Like Identity for Deformed Paths

In the DCIM approach, the core of the algorithm is to approximate a spectral-domain Green's function with a linear combination of rational functions containing exponentials. The conventional algorithm involves the computation of the exponents, through a subspace approach such as the general pencil of function (GPOF) [33] or ESPRIT [34], and the computation of the weights of the corresponding exponentials by using OLS. However, the (unweighted) energy minimization in the spectral-domain, as enforced by the OLS step, is not equivalent to energy minimization in the spatial domain. For this reason, in this section, the spectral-domain equivalent of the spatial-domain error criterion given in (5) is to be obtained so that the spectral-domain approximation could be executed in a spatially meaningful way.

The spectral-domain equivalent of the metric in (5) can be obtained by substituting the definition of the Hankel transform (1) into (5) as

$$\begin{aligned} C_2(e) &= \int_0^\infty w(\rho) e(\rho) e^*(\rho) d\rho \\ &= \frac{1}{4\pi^2} \int_S \int_S E(k_{\rho_1}) E(k_{\rho_2})^* K(k_{\rho_1}, k_{\rho_2}) \\ &\quad \times k_{\rho_1} k_{\rho_2}^* dk_{\rho_1} dk_{\rho_2}^* \end{aligned} \tag{6}$$

where

$$K(k_{\rho_1}, k_{\rho_2}) = \int_0^\infty w(\rho) J_0(k_{\rho_1}) J_0^*(k_{\rho_2}) d\rho. \tag{7}$$

Note that the change of the order of integration in obtaining the final expression in (6) can be justified by the uniform convergence arguments supported by the choice of the weighting function $w(\rho)$ [35]. As a special case, when the weighting function is selected as

$$w(\rho) = \begin{cases} \rho, & 0 \leq \rho \leq R \\ 0, & \text{otherwise} \end{cases} \tag{8}$$

the integration kernel K in (7) can be simplified to

$$L_R(k_{\rho_1}, k_{\rho_2}) = \int_0^R \rho J_0(k_{\rho_1}) J_0(k_{\rho_2}^*) d\rho \tag{9}$$

which is known as the Lommel integral [36], and has a closed-form expression as

$$\begin{aligned} &L_R(k_{\rho_1}, k_{\rho_2}) \\ &= \begin{cases} \frac{1}{k_{\rho_1}^2 - k_{\rho_2}^2} (k_{\rho_2} J_0(k_{\rho_1} R) J_0^*(k_{\rho_2} R) \\ \quad - k_{\rho_1} J_0(k_{\rho_2} R) J_0^*(k_{\rho_1} R)), & k_{\rho_1} \neq k_{\rho_2} \\ \frac{k_{\rho_1}^2}{2} (J_0^2(k_{\rho_1} R) + J_1^2(k_{\rho_1} R)), & k_{\rho_1} = k_{\rho_2}. \end{cases} \end{aligned} \tag{10}$$

In the DCIM approach, the numerical approximation is performed over a discrete set of frequencies, as specified by the set $\mathcal{K} = \{k_\rho^{(1)}, k_\rho^{(2)}, \ldots, k_\rho^{(N)}\}$. Therefore, the spectral-domain metric in (6) can be approximately evaluated as follows:

$$\begin{aligned} \mathcal{C}_\mathcal{K}(E) &= \frac{1}{4\pi^2} \mathbf{E}^H \mathbf{\Gamma}_\mathcal{K} \mathbf{E} \\ &= \frac{1}{4\pi^2} \sum \sum_{k_{\rho_1}, k_{\rho_2} \in \mathcal{K}} E(k_{\rho_1}) E^*(k_{\rho_2}) K(k_{\rho_1}, k_{\rho_2}) \\ &\quad \times k_{\rho_1} k_{\rho_2}^* \Delta_{k_{\rho_1}} \Delta_{k_{\rho_2}}^* \end{aligned} \tag{11}$$

where $\mathbf{E}$ is a vector containing the spectral-domain error values as

$$\mathbf{E} = \left[E\left(k_\rho^{(1)}\right) \quad E\left(k_\rho^{(2)}\right) \quad \ldots \quad E\left(k_\rho^{(N)}\right) \right]^T \tag{12}$$

$\mathbf{\Gamma}_{\mathcal{K}}$ is an $N \times N$ matrix, whose element at row m and column n is given by

$$\Gamma_{mn} = {k_\rho}^{(n)} {k_\rho}^{(m)^*} \Delta_{{k_\rho}^{(n)}} \Delta^*_{{k_\rho}^{(m)}} K\left({k_\rho}^{(n)}, {k_\rho}^{(m)}\right) \tag{13}$$

and $\Delta_{{k_\rho}^{(n)}}$ is the (backward or forward) difference of the spectral grid sequence evaluated at ${k_\rho}^{(n)}$.

Remembering that, for a positive definite matrix $\mathbf{W}$, the weighted 2-norm is defined in general as

$$\|\mathbf{x}\|_{\mathbf{W}} \triangleq \sqrt{\mathbf{x}^H \mathbf{W} \mathbf{x}}. \tag{14}$$

The spectral-domain reflection of the weighted error metric in the spatial-domain becomes equivalent to a squared weighted 2-norm

$$\mathcal{C}_{\mathcal{K}}(E) = \frac{1}{4\pi^2} \|\mathbf{E}\|^2_{\mathbf{\Gamma}_{\mathcal{K}}} \tag{15}$$

as $\mathbf{\Gamma}_{\mathcal{K}}$ is a Hermitian (positive definite) weighting matrix. Since it is only a function of the spectral-domain grid points, which are known *a priori* depending upon the choice of the paths in the DCIM implementation, it can be precalculated for once and employed in all other computations. Consequently, in order to incorporate the spatial-domain error criterion into the DCIM algorithm, the weighted least squares (WLS) approach with the weighting matrix $\mathbf{\Gamma}_{\mathcal{K}}$ needs to replace the OLS used in the conventional approach. This would cause the spectral shaping of the errors in favor of the desired spatial performance.

For multilevel DCIM algorithms, the integration path in the spectral domain is divided into multiple connected regions, on each of which the DCIM algorithm is applied separately. Since the weighting matrix is formed from the spectral grid, as described in (13), its diagonal sub-matrices correspond to the subregions of the spectral grid, and therefore, they should be used as the weighting matrices for the corresponding regions. For example, for the three-level DCIM [37], the set $\mathcal{K}$ can be written as the union of three disjoint (ordered) sets, in the form of

$$\mathcal{K} = \mathcal{K}_1 \bigcup \mathcal{K}_2 \bigcup \mathcal{K}_3 \tag{16}$$

where $\mathcal{K}_i$ denotes the set of spectral points for Region-i, with cardinality n_i. In this case, the weighting matrix $\mathbf{\Gamma}_{\mathcal{K}}$ can be partitioned as

$$\mathbf{\Gamma}_{\mathcal{K}} = \begin{bmatrix} \mathbf{\Gamma}_{\mathcal{K}_1} & \mathbf{\Gamma}_{\mathcal{K}_1,\mathcal{K}_2} & \mathbf{\Gamma}_{\mathcal{K}_1,\mathcal{K}_3} \\ \mathbf{\Gamma}^H_{\mathcal{K}_1,\mathcal{K}_2} & \mathbf{\Gamma}_{\mathcal{K}_2} & \mathbf{\Gamma}_{\mathcal{K}_2,\mathcal{K}_3} \\ \mathbf{\Gamma}^H_{\mathcal{K}_1,\mathcal{K}_3} & \mathbf{\Gamma}^H_{\mathcal{K}_2,\mathcal{K}_3} & \mathbf{\Gamma}_{\mathcal{K}_3} \end{bmatrix} \tag{17}$$

and, for Region-i, the sub-matrix $\mathbf{\Gamma}_{\mathcal{K}_i}$ is to be used as the weighting matrix in the implementation of WLS.

B. Practical Application

Once the mapping of the error criterion from the spatial to spectral domain has been established by introducing a proper WLS, for its practical application, the only thing left is the judicious choice of weighting function $w(\rho)$ in (5). As was demonstrated in Section III-A, the choice of linear weighting over a window (8) seems to be quite convenient, referred to as Metric-1 throughout this work, as it results in a weighting matrix that can be written in terms of the kernel function L_R in the form of

$$\Gamma_{mn} = {k_\rho}^{(n)} {k_\rho}^{(m)^*} \Delta_{{k_\rho}^{(n)}} \Delta^*_{{k_\rho}^{(m)}} L_R\left({k_\rho}^{(n)}, {k_\rho}^{(m)}\right) \tag{18}$$

where L_R has a closed-form expression (10). However, such a convenience would not be enough if the choice of the weighting function were not suitable for the type of functions to be approximated, namely, Green's functions in layered media. That is, the choice of the weighting function needs to take into consideration the asymptotic behavior of the function to be approximated, otherwise, undue weight may be given to rather less significant parts of the function, possibly leading to an erroneous estimate of the function. Since surface waves are the slowest decaying wave components of Green's functions in planar layered media, with the rate of $\rho^{-1/2}$, the relative biasing of the error for large distances requires a linear weighting function for the weighted error energy (5). Therefore, in addition to its algebraic convenience, the asymptotic nature of the functions to be approximated also justifies the use of such weighting functions.

However, in the numerical implementation of (10), especially for relatively large values of the radius R, the arguments of Bessel functions may grow to an extent that the values of Bessel functions may not be reliable, and as a result, the resulting error may cause critical inaccuracies in (10) due to the ill-conditioned subtraction process. In order to circumvent this numerical problem, a simple approximation for the weighting $\mathbf{\Gamma}_{\mathcal{K}}$ can be proposed (referred to as Metric-2) as follows: if row-i (or column-i) of $\mathbf{\Gamma}_{\mathcal{K}}$ requires the evaluation of a Bessel function with an argument greater than a chosen threshold $\tau_{\rm th}$, then all the elements in row- and column-i are set to 0, except

$$\Gamma_{ii} = \mathcal{R}e\left\{{k_\rho}^{(i)}\right\} \mathcal{R}e\left\{\Delta_{{k_\rho}^{(i)}}\right\}. \tag{19}$$

This approximation on the entries of the weighting matrix $\mathbf{\Gamma}$ is justified by the following identity [38]:

$$\int_0^\infty \rho J_0(\alpha\rho) J_0(\beta\rho) d\rho = \frac{1}{\alpha} \delta(\alpha - \beta). \tag{20}$$

As an alternative approach, one can use the Parseval identity for the Hankel transform (Metric-3),

$$\int_0^\infty \rho |e(\rho)|^2 d\rho = \frac{1}{4\pi^2} \int_0^\infty k |E(k)|^2 dk \tag{21}$$

which is valid for cases where the integration path aligns with the real axis in the spectral domain. For the cases where the integration path S does not align with the real axis, it could be approximated as

$$\int_0^\infty \rho |e(\rho)|^2 d\rho \approx \frac{1}{4\pi^2} \int_S |E(k_\rho)|^2 \mathcal{R}e\{k_\rho\} \mathcal{R}e\{dk_\rho\} \tag{22}$$

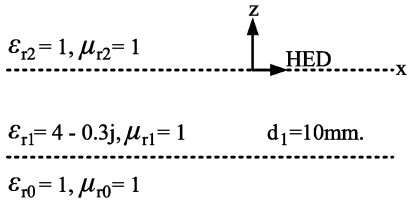

Fig. 2. Lossy material in air. The locations of the observation and the horizontal electric dipole (HED) are at the interface between the air and the upper boundary of the dielectric layer.

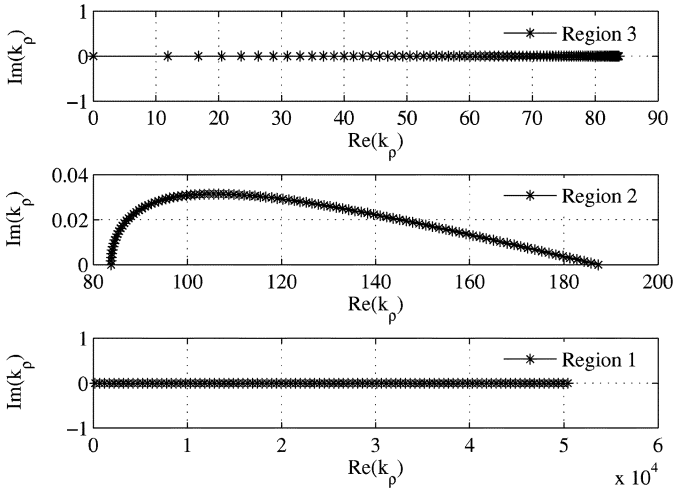

Fig. 3. Integration path for the three-level DCIM on complex k_ρ-plane.

which can be justified by the closeness of the integration path to the real axis. The spectral-domain weighting matrix corresponding to this case can be written as

$$\mathbf{\Gamma}_{\mathcal{K}} = \mathrm{diag}\Big(\Big[\mathcal{R}e\left\{{k_\rho}^{(1)}\right\}\mathcal{R}e\left\{\Delta_{{k_\rho}^{(1)}}\right\} \mathcal{R}e\left\{{k_\rho}^{(2)}\right\}\mathcal{R}e\left\{\Delta_{{k_\rho}^{(2)}}\right\}\ldots \mathcal{R}e\left\{{k_\rho}^{(N)}\right\}\mathcal{R}e\left\{\Delta_{{k_\rho}^{(N)}}\right\}\Big]\Big). \quad (23)$$

Note that although there is no spatial selectivity, when compared to the weighting matrices of Metric-1 and Metric-2, as given in (18) and (19), respectively, it is a convenient choice because of its computational efficiency.

In order to assess the performance of the proposed three different implementations of the spectral-domain weighted energy, namely, Metric-1, Metric-2, and Metric-3, Green's functions in the spectral and spatial domains are obtained for a lossy slab with $\epsilon_r = 4 - j0.3$ in air at 4 GHz (Fig. 2). The spatial-domain Green's functions are obtained from their spectral-domain counterparts by using the three-level DCIM, where the integration path S is divided into three sub-regions such that they all pass very close to the real axis, as shown in Fig. 3. Based on this geometry and the choice of the path, Fig. 4 shows the estimates of the spatial-domain weighted energy obtained by the three different spectral-domain implementations (18), (19), and (23), and compares them with the true value obtained from the spatial-domain implementation of the metric (5) with the weighting function (8) via numerical integration. While Metric-1 employs

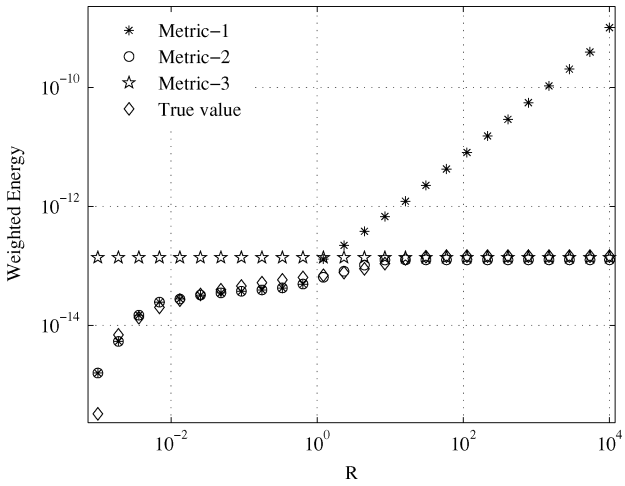

Fig. 4. Spatial-domain weighted energy and its estimates via three different metrics.

a Parseval-like identity, Metric-2 modifies this approach by introducing a threshold for distance and Metric-3 uses the Parseval identity as if the integration path aligns with the real axis in the spectral domain. It is observed from Fig. 4 that the spatial-domain estimate of the weighted energy by Metric-1 is not reliable for large values of R as expected. On the other hand, Metric-2 and Metric-3 seem to have fixed the problem and the weighted energy obtained via these metrics converge to the true value for large R values. As a result of this assessment, in addition to comparing computational efficiency of the metrics, Metric-3 is chosen and employed throughout this work to minimize the spatial-domain weighted error energy of Green's functions approximated by the DCIM.

C. DCIM With Spatial Error Criterion

Based on the discussion in Section III-B about bridging the spatial- and spectral-domain metrics, the details of the DCIM with the spatial-domain error criterion, as applied to Green's functions, are provided in this section.

The DCIM for Green's functions is based on the approximation of the spectral-domain Greens functions in terms of a special class of functions as

$$G_a(k_\rho) = \sum_{l=1}^{M} \alpha^{(l)} \frac{e^{-\beta^{(l)} k_z}}{jk_z} \quad (24)$$

where M is the number of fractional terms containing exponentials used in the approximation, $\beta^{(l)}$'s are the constants of the exponents, and $\alpha^{(l)}$'s are the weights of the fractional terms. The goal is to choose the parameters $\boldsymbol{\beta}$ and $\boldsymbol{\alpha}$ to minimize

$$\|\mathbf{G} - \mathbf{G}_a\|^2_{\mathbf{\Gamma}_{\mathcal{K}}} \quad (25)$$

where $\mathbf{G}$ is the vector containing the samples of the spectral-domain Green's function and $\mathbf{G}_a$ is the vector containing the samples of the corresponding approximation function. This optimization setting is a nonlinear least squares problem, and as such it is computationally quite expensive. Therefore, in the implementation of the DCIM, the constant parameters $\boldsymbol{\beta}$ and $\boldsymbol{\alpha}$ are obtained in separate steps: first, a subspace-based approach,

such as GPOF or ESPRIT methods, is applied to $H(k_\rho) = jk_zG(k_\rho)$ to obtain the constant parameters of the exponents $\boldsymbol{\beta}$, and then, an optimization procedure is employed to get the weight parameters $\boldsymbol{\alpha}$. Since the first step involves a nonlinear approximation, the error criterion is introduced into the second step, i.e., into the calculation of the weight parameters. Therefore, to elucidate the difference between the traditional use of the DCIM and the proposed one, the main steps of the computation of the weight parameters in both approaches are provided below.

In the traditional DCIM, the weight parameters $\boldsymbol{\alpha}$ are computed as the solution of the OLS problem

$$\text{minimize}\|\mathbf{H}-\mathbf{H}_a\|^2 \tag{26}$$

where

$$\mathbf{H}=\left[H\left(k_\rho{}^{(1)}\right)\ H\left(k_\rho{}^{(2)}\right)\ \ldots\ H\left(k_\rho{}^{(N)}\right)\right]^T \tag{27}$$

$$H\left(k_\rho{}^{(n)}\right)=2jk_z{}^{(n)}G(k_\rho{}^{(n)}),\qquad n=1,\ldots,N \tag{28}$$

and

$$\mathbf{H}_a=\left[H_a\left(k_\rho{}^{(1)}\right)\ H_a\left(k_\rho{}^{(2)}\right)\ \ldots\ H_a\left(k_\rho{}^{(N)}\right)\right]^T \tag{29}$$

$$\begin{aligned}H_a\left(k_\rho{}^{(n)}\right)&=2jk_z{}^{(n)}G_a\left(k_\rho{}^{(n)}\right)\\&=\sum_{l=1}^{M}\alpha^{(l)}e^{-\beta^{(l)}k_z{}^{(n)}},\qquad n=1,\ldots,N.\end{aligned} \tag{30}$$

Therefore, $\alpha^{(l)}$'s are obtained by matching the jk_z-scaled version of the spectrum via the solution of the OLS problem as

$$\boldsymbol{\alpha}_{\text{OLS}}=\mathbf{A}^{\dagger}\mathbf{H} \tag{31}$$

where $\mathbf{A}^{\dagger}$ is the Moore–Penrose pseudoinverse of $\mathbf{A}$, and

$$\mathbf{A}=\begin{bmatrix}e^{-\beta^{(1)}k_z{}^{(1)}} & e^{-\beta^{(2)}k_z{}^{(1)}} & \cdots & e^{-\beta^{(M)}k_z{}^{(1)}}\\ e^{-\beta^{(1)}k_z{}^{(2)}} & e^{-\beta^{(2)}k_z{}^{(2)}} & \cdots & e^{-\beta^{(M)}k_z{}^{(2)}}\\ \vdots & \vdots & \cdots & \vdots\\ e^{-\beta^{(1)}k_z{}^{(N)}} & e^{-\beta^{(2)}k_z{}^{(N)}} & \cdots & e^{-\beta^{(M)}k_z{}^{(N)}}\end{bmatrix}. \tag{32}$$

However, for the proposed DCIM algorithm, the weight parameters $\alpha^{(l)}$'s are obtained from the solution of the WLS problem, whose formal statement is given as

$$\text{minimize}\|\mathbf{G}-\mathbf{G}_a\|^2_{\boldsymbol{\Gamma}_{\mathcal{K}}} \tag{33}$$

and its solution can be compactly written as

$$\boldsymbol{\alpha}_{\text{WLS}}=\left(\boldsymbol{\Gamma}_{\mathcal{K}}^{1/2}\mathbf{B}\right)^{\dagger}\left(\boldsymbol{\Gamma}_{\mathcal{K}}^{1/2}\mathbf{G}\right) \tag{34}$$

where

$$\mathbf{B}=\begin{bmatrix}\frac{e^{-\beta^{(1)}k_z{}^{(1)}}}{2jk_z{}^{(1)}} & \frac{e^{-\beta^{(2)}k_z{}^{(1)}}}{2jk_z{}^{(1)}} & \cdots & \frac{e^{-\beta^{(M)}k_z{}^{(1)}}}{2jk_z{}^{(1)}}\\ \frac{e^{-\beta^{(1)}k_z{}^{(2)}}}{2jk_z{}^{(2)}} & \frac{e^{-\beta^{(2)}k_z{}^{(1)}}}{2jk_z{}^{(2)}} & \cdots & \frac{e^{-\beta^{(M)}k_z{}^{(2)}}}{2jk_z{}^{(2)}}\\ \vdots & \vdots & \cdots & \vdots\\ \frac{e^{-\beta^{(1)}k_z{}^{(N)}}}{2jk_z{}^{(N)}} & \frac{e^{-\beta^{(2)}k_z{}^{(N)}}}{2jk_z{}^{(N)}} & \cdots & \frac{e^{-\beta^{(M)}k_z{}^{(N)}}}{2jk_z{}^{(N)}}\end{bmatrix} \tag{35}$$

and $\boldsymbol{\Gamma}_{\mathcal{K}}^{1/2}$ is a matrix square root of $\boldsymbol{\Gamma}_{\mathcal{K}}$ satisfying $\boldsymbol{\Gamma}_{\mathcal{K}}^{1/2^H}\boldsymbol{\Gamma}_{\mathcal{K}}^{1/2}=\boldsymbol{\Gamma}_{\mathcal{K}}$.

In summary, the proposed DCIM approach with the spatial-domain error criterion has two major differences from the conventional DCIM approach in obtaining the weight parameters $\alpha^{(l)}$'s, which are: 1) the use of the WLSs instead of the OLS and 2) fitting directly the spectral-domain function $G(k_\rho)$ rather than its scaled version $H(k_\rho)$.

D. Improvement for the Multilevel DCIM

In addition to incorporating the spatial-domain error criterion into the DCIM, there is another source of improvement for the multilevel DCIM approach. In a typical multilevel applications, the domain over which the spectral-domain function is sampled is divided into sub-regions, which are processed in order, starting from the highest end of the spectrum to the lowest end. The DCIM procedure outlined in Section III-C is applied to each region, but their implementations are not independent: once the fitting parameters for Region-l are obtained, the corresponding exponentials are subtracted from the original function used for Region-l in order to get the function to be approximated over the subsequent regions. Therefore, the multilevel DCIM algorithm based on this exponential peeling has the basic advantage that the number of spectral-domain samples required for the whole process and their processing costs by the DCIM are greatly reduced. However, this causally semi-independent processing of the subregions has the basic problem of leakage from regions with larger indices to regions with smaller indices.

In order to alleviate this leakage problem, the whole DCIM algorithm is implemented as usual, except the final (weighted) least squares optimization that provides the weight parameters for the last region. At this stage, all the weight parameters computed in the previous steps are completely ignored, and a fresh (weighted) least squares optimization is applied, over all or a part of the spectral samples that were already used, to obtain the weight parameters for all the exponentials found by the multilevel procedure. This approach makes use of the fact that while the subspace-based frequency estimation step (GPOF or ESPRIT) requires uniformly spaced samples, there is no such requirement for the least squares applications.

IV. Numerical Examples and Discussions

A. Link Between Spectral and Spatial Domains

Recall that the motivation of this study is to achieve spatial-domain error minimization from the spectral-domain processing. Since minimizing the 2-norm in the Hankel transform domain is not equivalent to minimizing the 2-norm in the spatial domain, the use of OLS in the spectral domain, which is the case in the standard DCIM applications, may not achieve the spatial-domain error minimization. To illustrate this fact, the standard and proposed three-level DCIM algorithms were employed to find the vector-potential Green's function for the geometry and the path of integration given in Figs. 2 and 3, respectively. Since one needs to settle on the number of exponentials M_i to express the signal in each region, where i represents the region for the multilevel DCIM, for the example, the

TABLE I
ERROR AND ENERGY (E) OF THE SPATIAL- AND SPECTRAL-DOMAIN GREEN'S FUNCTIONS ESTIMATED BY THE STANDARD AND PROPOSED THREE-LEVEL DCIM FOR CASE-1

Case-1 (3-5-5)	Proposed DCIM		Standard DCIM	
	Spectral	Spatial	Spectral	Spatial
Error	1.63E-15	8.54E-15	1.23E-15	1.03E-10
E-True Signal	1.38E-13	1.46E-13	2.52E-14	0.00117558
E-Fitting Signal	1.36E-13	1.48E-13	2.23E-14	0.00117544

TABLE II
ERROR AND ENERGY (E) OF THE SPATIAL- AND SPECTRAL-DOMAIN GREEN'S FUNCTIONS ESTIMATED BY THE STANDARD AND PROPOSED THREE-LEVEL DCIM FOR CASE-2

Case-2 (3-5-7)	Proposed DCIM		Standard DCIM	
	Spectral	Spatial	Spectral	Spatial
Error	1.65E-15	1.55E-14	1.12E-15	1.66E-10
E-True Signal	1.38E-13	1.46E-13	2.52E-14	0.00117558
E-Fitting Signal	1.36E-13	1.48E-13	2.22E-14	0.00117526

following two cases were used to obtain the spectral- and spatial-domain errors in the fitting by the standard and proposed three-level DCIM: *case-1:* $M_1 = 3, M_2 = 5, M_3 = 5$ and *case-2:* $M_1 = 3, M_2 = 5, M_3 = 7$, as given in Tables I and II, respectively. In comparing the two cases, the aim is to demonstrate whether the improvement or deterioration in the spatial-domain error is mapped onto the spectral-domain error consistently. Note that while the true function in the spectral domain corresponds to the closed-form expression, the true function in the spatial domain is obtained by the numerical integration of (1).

Examining the results of the standard DCIM in Tables I and II, it is observed that while the OLS fitting error of *Case-1* is greater than the error of *Case-2* in the spectral domain, the error of *Case-1* is smaller than the error of *Case-2* in the spatial domain. It shows that under the same number of samples, when the number of complex images is changed, the increase (decrease) in the spectral-domain error does not necessarily imply an increase (decrease) in the spatial-domain error for the OLS fitting. This is due to the fact that the spectral-domain fitting in the standard DCIM is performed without a correct link to the spatial domain. Since only spectral-domain information is available in reality, the user unwittingly chooses Case-2 as a better fitting. However, for the proposed DCIM, the consistency between the errors in the spectral and spatial domain is achieved by the weighted energy minimization in the spectral domain, which is equivalent to the weighted energy minimization in the spatial domain, as can be observed from Tables I and II: The WLS fitting error of *Case-1* is smaller than the error of *Case-2* both in the spectral and spatial domains. In addition to the error values, the values of the signal energies obtained by the standard DCIM are quite different for the spatial and spectral domains, which contradicts the Parseval-like relation of the signals, whereas the energies of the signals in the two domains are very close in the case of the proposed DCIM, as they should.

B. Verification of the Proposed Method

In this section, some numerical examples are provided to assess and to validate the proposed DCIM for its ability to control errors in the spatial domain, as well as in the spectral domain. For the sake of coherence in the discussions, the same example used in the previous sections is employed (Fig. 2), and for the sake of brevity in the presentation, only the vector potential Green's function in the spatial domain, as obtained from the standard and proposed DCIM, are presented and compared with those obtained by the numerical integration of its spectral-domain counterpart (Fig. 5). A few notes on the chosen geometry and Green's function for the example are in order, which are: 1) the proposed method has been successfully applied to many geometries for all components of Green's dyadic of the vector potential and the Green's functions of the scalar potentials; 2) the geometry has a surface wave pole (SWP), but since the slab is lossy, its contribution decays exponentially in the far-field region, resulting in a dominating lateral wave component in that region; and 3) although SWPs are generally extracted *a priori* in the application of the multilevel DCIM, as suggested in [31], they are not extracted in this example just to see their influence on the approximation. Before introducing the results and accompanying discussions, it would be instructive to

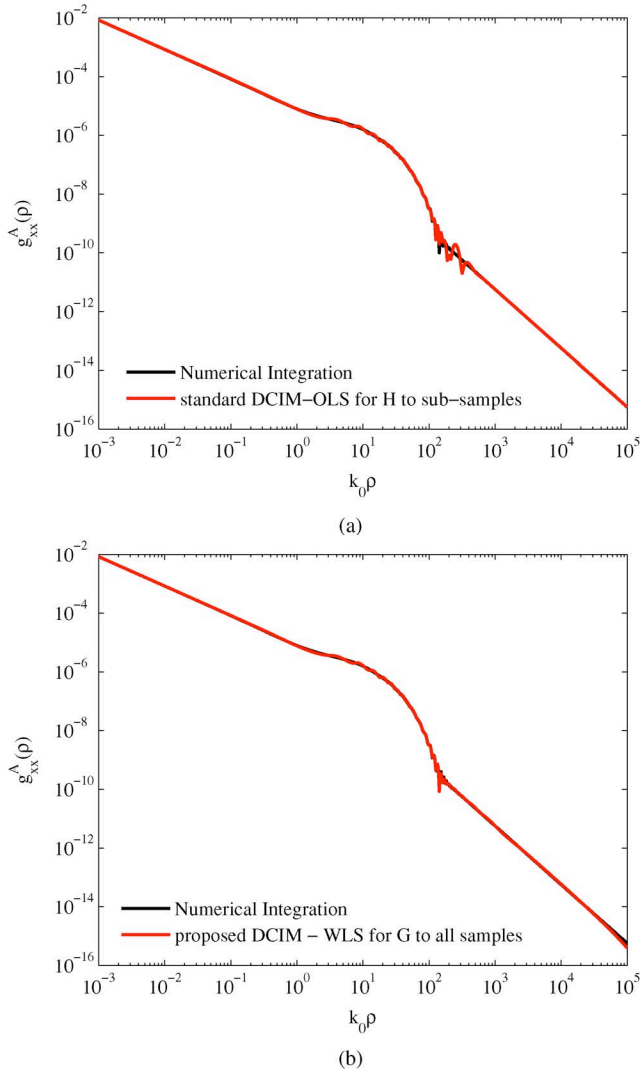

Fig. 5. Magnitude of the spatial-domain Green's function for the vector potential obtained by the: (a) standard DCIM and (b) proposed DCIM. The numerical integration result is presented for verification. Parameters of the geometry are given in Fig. 2 and the frequency of operation is 4 GHz.

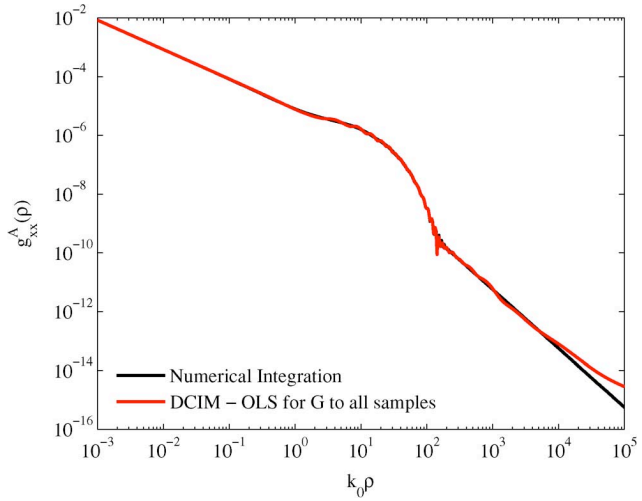

Fig. 6. Magnitude of the spatial-domain Green's function for the vector potential. Parameters of the geometry are given in Fig. 2 and the frequency of operation is 4 GHz.

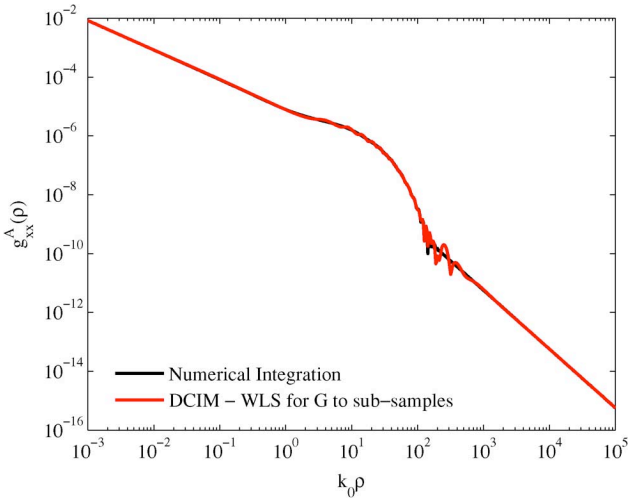

Fig. 7. Magnitude of the spatial-domain Green's function for the vector potential. Parameters of the geometry are given in Fig. 2 and the frequency of operation is 4 GHz.

first recall the following major differences between the proposed DCIM approach with the spatial-domain error criterion and the standard DCIM approach:

- use of the WLS, instead of using the ordinary least squares (WLS versus OLS);
- direct fitting of the spectral-domain function $G(k_\rho)$, instead of its scaled version $H(k_\rho)$ (G versus H);
- applying the final WLS optimization to all spectral samples to obtain all the weight parameters, instead of obtaining the weight parameters of each region separately (all samples versus sub-samples).

As the first example, the spatial-domain Green's function for the vector potential is presented, which is obtained from the standard DCIM, and the proposed DCIM with all other improvements [see Fig. 5(a) and (b), respectively]. Note that all the results obtained throughout this work are compared to the one obtained by the numerical integration of the spectral-domain Green's functions (1). After a brief study on the magnitudes of the spatial-domain Green's function in Figs. 5, it is quite clear that both approaches perform quite satisfactorily as far as the accuracy of the results are concerned. However, the slight oscillations around the region where the lateral wave begins to dominate are completely eliminated by the proposed DCIM, predicting the true nature of the Green's function better than the standard DCIM.

To assess the sole contribution of the WLS optimization, and the influence of the additional improvements, to the final result, these improvements are also employed with the standard DCIM. To equalize the effects of the second and third proposed differences stated above, the conventional application of the standard DCIM is modified to the use of the OLS optimization with the spectral-domain function $G(k_\rho)$ over all samples, instead of its scaled version $H(k_\rho)$ over the sub-samples corresponding to the individual regions of the multilevel algorithm. It is observed from Fig. 6 that although the results obtained by the modified version of the standard DCIM have been improved in the middle, where the lateral wave begins to dominate, as compared with the results presented in Fig. 5(a), they deteriorate at the far end, as compared to those obtained by the proposed DCIM [see Fig. 5(b)]. As a result, improvements on the leakage and on the implementation of the method to the actual function rather than its scaled version have resulted in some improvements in the intermediate region, which seems to be at the expense of the results in the very far region. To distinguish the effects of the leakage in this work, the region-specific weight parameters are used to calculate the spatial-domain Green's function during the implementation of the proposed DCIM, i.e., the leakage alleviation is not performed. It is observed from Fig. 7 that the resulting spatial-domain Green's function exhibits some oscillatory behavior in the middle, and can safely be attributed to the leakages between the subregions.

C. More About the Leakage

As discussed in Section IV-B, the proposed DCIM brings in significant improvements to the multilevel fitting not only by introducing WLS to incorporate the spatial-domain error criterion, but also by eliminating the possible leakages. In this section, the leakage problem in a standard multilevel DCIM is discussed over the same example that was examined in the previous sections.

In the three-level DCIM, the spectral-domain sample points are split into three sets, and the approximation is performed over these sets to obtain the corresponding approximating functions, i.e., exponentials, with their exponents and coefficients. During the process, once the fitting parameters for Region-1 are obtained, the corresponding exponentials are subtracted from the original function, and the resulting function is used for the approximation in Region-2. Following that, the fitting parameters for Region-2 are obtained and the corresponding exponentials are subtracted from the previous function over Region-3. Finally, fitting in Region-3 is performed. Wherever this idea of exponential peeling is applied, it simply assumes that the function calculated by the parameters found from the fitting in Region-2 is 0 in Region-1, and similarly, the function calculated by the parameters found from the fitting in Region-3 is 0 in Region-2 and Region-1. However, since there is no enforcement in

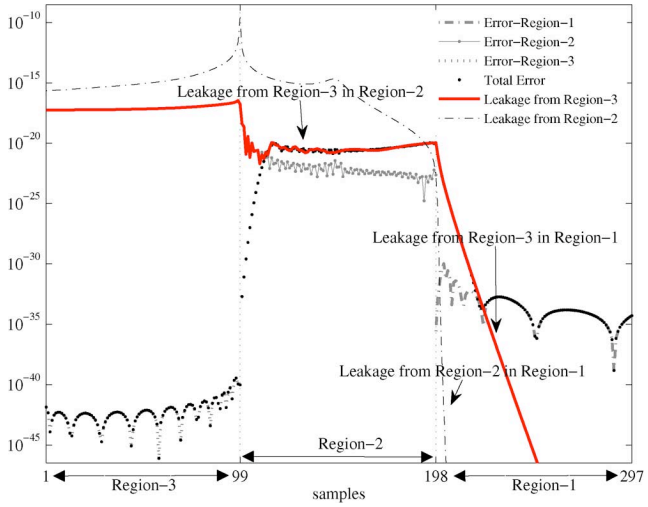

Fig. 8. Demonstration of the leakage: leakage from Region-2 to Region-1, leakage from Region-3 to Region-2 and to Region-1, the region specific errors and the overall error for the standard DCIM. Parameters of the geometry are given in Fig. 2 and the frequency of operation is 4 GHz.

the algorithm to guarantee these assumptions, the leakage from regions of low frequencies to the regions of high frequencies may occur, as shown in Fig. 8, where different error calculations are presented in the spectral domain. As Fig. 8 seems to be quite complicated, to make it comprehensible, the curves in the figure are explained as follows.

1) The curves designated as Error-Region-i $(i = 1,2,3)$ demonstrate region-specific errors defined as the square of the magnitude of the difference between the actual function and its approximation over the samples of the region.
2) The curve designated as Total Error is calculated as the square of the magnitude of the difference between the overall Green's function and its fitting.
3) The curve designated as Leakage from Region-2 is the sum of the complex exponentials whose parameters are obtained from the fitting in Region-2.
4) The curve designated as Leakage from Region-3 is the sum of the complex exponentials whose parameters are obtained from the fitting in Region-3.

As it is observed, the leakages exist and leakage from Region-3 is highly dominant, especially in Region-2. In fact, it is so dominant that the overall error follows the leakage even if the actual fitting error in Region-2 is smaller. This matter continues in Region-1 as well, until the leakage from Region-3 becomes smaller than Error-region-1. That is why taking the region specific error values as the error criterion may lead to incorrect conclusions about that fitting.

V. Conclusion

After the three-level DCIM that can take different wave natures into account was recently introduced, the spatial-domain Green's functions was successfully approximated in closed forms for all ranges and materials [31]. However, even with this development, the DCIM approach may not be considered suitable for the development of commercial EM-based simulation tools for planar layered structures. The main reason for this is the lack of an error metric that could be incorporated into the algorithm to ensure the accuracy of the end result within the prescribed limits. It is demonstrated that the metric introduced in this work can be easily implemented to any DCIM approach, which is very likely to boost the confidence of the method. A suitable and convenient metric is proposed by mapping the error criterion from the spatial to spectral domains via introducing a proper WLS (with a linear weighting function over a window) into the standard DCIM algorithm. In addition, the leakage problem that is inherent to the standard DCIM implementation has also been addressed and remedied. Modifying the standard DCIM, by implementing the minor improvements (elimination of leakage and direct fitting of the spectral-domain function) together with the major contribution of this work, i.e., incorporating the spatial-domain error criterion, has resulted in a robust, accurate, and very reliable DCIM algorithm. The method was successfully applied to many different geometries and different components of the Green's functions.

References

[1] R. F. Harrington, *Field Computation by Moment Methods*. Melbourne, FL: Krieger, 1982.
[2] W. C. Chew, *Waves and Fields in Inhomogeneous Media*. New York: Van Nostrand, 1990.
[3] N. Kinayman and M. I. Aksun, *Modern Microwave Circuits*. Norwood, MA: Artech House, 2005.
[4] J. R. Mosig, "Arbitrarily shaped microstrip structures and their analysis with a mixed potential integral equation," *IEEE Trans. Microw. Theory Tech.*, vol. 36, no. 2, pp. 314–323, Feb. 1988.
[5] L. Alatan, M. I. Aksun, K. Mahadevan, and T. Birand, "Analytical evaluation of the MoM matrix elements," *IEEE Trans. Microw. Theory Tech.*, vol. 44, no. 4, pp. 519–525, Apr. 1996.
[6] M. J. Tsai, F. D. Flavis, O. Fordharn, and N. G. Alexopoulos, "Modeling planar arbitrarily shaped microstrip elements in multilayered media," *IEEE Trans. Microw. Theory Tech.*, vol. 45, no. 3, pp. 330–337, Mar. 1997.
[7] M. R. Abdul-Gaffoor, H. K. Smith, A. A. Kishk, and A. W. Glisson, "Simple and efficient full-wave modeling of electromagnetic coupling in realistic RF multilayer PCB layouts," *IEEE Trans. Microw. Theory Tech.*, vol. 50, no. 6, pp. 1445–1457, Jun. 2002.
[8] T. Onal, M. I. Aksun, and N. Kinayman, "A rigorous and efficient analysis of 3-D printed circuits: Vertical conductors arbitrarily distributed in multilayer environment," *IEEE Trans. Antennas Propag.*, vol. 55, no. 12, pp. 3726–3729, Dec. 2007.
[9] J. R. Mosig and F. E. Gardiol, "A dynamical radiation model for microstrip structures," in *Advances in Electronics and Electron Physics*, P. W. Hawkes, Ed. New York: Academic, 1982, vol. 59, pp. 139–237.
[10] K. A. Michalski, "Extrapolation methods for Sommerfeld integral tails," *IEEE Trans. Antennas Propag.*, vol. 46, no. 10, pp. 1405–1418, Oct. 1998.
[11] D. G. Fang, J. J. Yang, and G. Y. Delisle, "Discrete image theory for horizontal electric dipoles in a multilayered medium," *Proc. Inst. Elect. Eng.*, vol. 135, no. 5, pp. 297–303, Oct. 1988.
[12] Y. L. Chow, J. J. Yang, D. G. Fang, and G. E. Howard, "A closed-form spatial Green's function for the thick microstrip substrate," *IEEE Trans. Microw. Theory Tech.*, vol. 39, no. 3, pp. 588–592, Mar. 1991.
[13] B. Hu and W. C. Chew, "Fast inhomogenous plane wave algorithm for electromagnetic solutions in layered media structures: Two-dimensional case," *Radio Sci.*, vol. 35, pp. 31–43, Jan.–Feb. 2000.
[14] N. Kinayman and M. I. Aksun, "Comparative study of acceleration techniques for integrals and series in electromagnetic problems," *Radio Sci.*, vol. 30, pp. 1713–1722, Nov.–Dec. 1995.
[15] M. I. Aksun and R. Mittra, "Derivation of closed-form Green's functions for a general microstrip geometry," *IEEE Trans. Microw. Theory Tech.*, vol. 40, no. 11, pp. 2055–2062, Nov. 1992.
[16] G. Dural and M. I. Aksun, "Closed-form Green's functions for general sources and stratified media," *IEEE Trans. Microw. Theory Tech.*, vol. 43, no. 7, pp. 1545–1552, Jul. 1995.
[17] M. I. Aksun, "A robust approach for the derivation of closed-form Green's functions," *IEEE Trans. Microw. Theory Tech.*, vol. 44, no. 5, pp. 651–658, May 1996.

[18] C. Tokgoz and G. Dural, "Closed-form Green's functions for cylindrically stratified media," *IEEE Trans. Microw. Theory Tech.*, vol. 48, no. 1, pp. 40–49, Jan. 2000.
[19] Y. Ge and K. P. Esselle, "New closed-form Green's functions for microstrip structures theory and results," *IEEE Trans. Microw. Theory Tech.*, vol. 50, no. 6, pp. 1556–1560, Jun. 2002.
[20] N. V. Shuley, R. R. Boix, F. Medina, and M. Horno, "On the fast approximation of Green's functions in MPIE formulations for planar layered media," *IEEE Trans. Microw. Theory Tech.*, vol. 50, no. 9, pp. 2185–2192, Sep. 2002.
[21] V. I. Okhmatovski and A. C. Cangellaris, "A new technique for the derivation of closed-form electromagnetic Green's functions for unbounded planar layered media," *IEEE Trans. Antennas Propag.*, vol. 50, no. 7, pp. 1005–1016, Jul. 2002.
[22] V. I. Okhmatovski and A. C. Cangellaris, "Evaluation of layered media Green's functions via rational function fitting," *IEEE Microw. Wireless Compon. Lett.*, vol. 14, no. 1, pp. 22–24, Jan. 2004.
[23] M. I. Aksun and G. Dural, "Clarification of issues on the closed-form Green's functions in stratified media," *IEEE Trans. Antennas Propag.*, vol. 53, no. 11, pp. 3644–3653, Nov. 2005.
[24] M. Yuan, T. K. Sarkar, and M. Salazar-Palma, "A direct discrete complex image method from the closed-form Green's functions in multilayered media," *IEEE Trans. Microw. Theory Tech.*, vol. 54, no. 3, pp. 1025–1032, Mar. 2006.
[25] V. N. Kourkoulos and A. C. Cangellaris, "Accurate approximation of Green's functions in planar stratified media in terms of a finite sum of spherical and cylindrical waves," *IEEE Trans. Antennas Propag.*, vol. 54, no. 5, pp. 1568–1576, May 2006.
[26] L. Zhuang, G. Zhu, Y. Zhang, and B. Xiao, "An improved discrete complex image method for Green's functions in multilayered media," *Microw. Opt. Technol. Lett.*, vol. 49, no. 6, pp. 1337–1340, 2007.
[27] R. R. Boix, F. Mesa, and F. Medina, "Application of total least squares to the derivation of closed-form Green's functions for planar layered media," *IEEE Trans. Microw. Theory Tech.*, vol. 55, no. 2, pp. 268–280, Feb. 2007.
[28] A. G. Polimeridis, T. V. Yioultsis, and T. D. Tsiboukis, "An efficient pole extraction technique for the computation of Green's functions in stratified media using a sine transformation," *IEEE Trans. Antennas Propag.*, vol. 55, no. 1, pp. 227–229, Jan. 2007.
[29] F. Mesa, R. R. Boix, and F. Medina, "Closed-form expressions of multilayered planar Green's functions that account for the continuous spectrum in the far field," *IEEE Trans. Microw. Theory Tech.*, vol. 56, no. 7, pp. 1601–1614, Jul. 2008.
[30] B. P. Wu and L. Tsang, "Fast computation of layered medium Green's functions of multilayers and lossy media using fast all-modes method and numerical modified steepest descent path method," *IEEE Trans. Microw. Theory Tech.*, vol. 56, no. 6, pp. 1446–1454, Jun. 2008.
[31] A. Alparslan, M. I. Aksun, and K. A. Michalski, "Closed-form Green's functions in planar layered media for all ranges and materials," *IEEE Trans. Microw. Theory Tech.*, vol. 58, no. 3, pp. 602–613, Mar. 2010.
[32] A. G. Polimeridis, T. V. Yioultsis, and T. D. Tsiboukis, "A robust method for the computation of Green's functions in stratified media," *IEEE Trans. Antennas Propag.*, vol. 55, no. 7, pp. 1963–1969, Jul. 2007.
[33] Y. Hua and T. K. Sarkar, "Generalized pencil-of-function method for extracting poles of an EM system from its transient response," *IEEE Trans. Antennas Propag.*, vol. 37, no. 2, pp. 229–234, Feb. 1989.
[34] A. Poulraj, R. Roy, and T. Kailath, "A subspace rotation approach to signal parameter estimation," *Proc. IEEE*, vol. 74, no. 7, pp. 1044–1045, Jul. 1986.
[35] T. M. Apostol, *Mathematical Analysis*. Reading, MA: Addison-Wesley, 1974.
[36] F. Bowman, *Introduction to Bessel Functions*. New York: Dover, 1958.
[37] A. Alparslan, "Study of Green's functions of potentials and fields in layered media composed of left-handed and rigth-handed materials," M.S. thesis, Dept. Elect. Electron. Eng., Koc Univ., Istanbul, Turkey, 2008.
[38] A. D. Polyanin and A. V. Manzhirov, *Handbook of Integral Equations*. Boca Raton, FL: CRC, 1998.

E. P. Karabulut (S'06) received the B.S. degree in electrical and electronics engineering from the Middle East Technical University, Ankara, Turkey, in 2004, the M.S. degree in electrical and computer engineering from Koc University, Istanbul, Turkey, in 2006, and is currently working toward the Ph.D. candidate n electrical engineering at Koc University, Istanbul, Turkey.

She is currently with the Department of Electrical and Electronics Engineering, Koc University, as a Research Assistant. Her research interests include numerical methods for electromagnetics, computational aspects of periodic structures including photonic-bandgap materials and metamaterials, and nanophotonics.

Ms. Karabulut was the recipient of a Scientific and Technological Research Council of Turkey (TUBITAK) Ph.D. Scholarship.

Alper T. Erdogan (M'00) was born in Ankara, Turkey, in 1971. He received the B.S. degree from the Middle East Technical University, Ankara, Turkey, in 1993, and the M.S. and Ph.D. degrees from Stanford University, Stanford, CA, in 1995 and 1999,, all in electrical engineering.

From September 1999 to November 2001, he was a Principal Research Engineer with the Globespan-Virata Corporation (formerly the Excess Bandwidth and Virata Corporations), Santa Clara, CA. Since January 2002, he has been an Assistant Professor with the Electrical and Electronics Engineering Department, Koc University, Istanbul, Turkey . His research interests include wireless and wireline communications, adaptive signal processing, optimization, system theory and control, and information theory.

Dr. Erdogan is an associate editor for the IEEE TRANSACTIONS ON SIGNAL PROCESSING. He was the recipient of the Scientific and Technological Research Council of Turkey (TUBITAK) Career Award (2005), the Werner Von Siemens Excellence Award (2007), the Turkish Academy of Sciences (TUBA) Outstanding Young Scientist Award (GEBIP) (2008), and TUBITAK Young Scientist Award (2010).

M. I. Aksun (M'92–SM'99) received the B.S. and M.S. degrees in electrical and electronics engineering from the Middle East Technical University, Ankara, Turkey, in 1981 and 1983, respectively, and the Ph.D. degree in electrical and computer engineering from the University of Illinois at Urbana-Champaign, in 1990.

From 1990 to 1992, he was a Post-Doctoral Fellow with the Electromagnetic Communication Laboratory, University of Illinois at Urbana-Champaign. From 1992 to 2001, he was a member of the Faculty of Electrical and Electronics Engineering with Bilkent University, Ankara, Turkey. In 2001, he was a member of the Faculty of Electrical and Electronics Engineering, Koc University, Istanbul, Turkey, as a Professor, and was the Dean of the College of Engineering (2004–2009). Since September 2009, he has been the Vice President for Research and Development with Koc University. His recent research interests include numerical methods for electromagnetics and optics, printed circuits and antennas, and nanophotonics.